This article was downloaded by: [Tomsk State University of Control Systems and Radio]
On: 19 February 2013, At: 12:13
Publisher: Taylor & Francis
Informa Ltd Registered in England and Wales Registered Number: 1072954 Registered office: Mortimer House, 37-41 Mortimer Street, London W1T 3JH, UK

Molecular Crystals and Liquid Crystals Incorporating Nonlinear Optics

Publication details, including instructions for authors and subscription information:
http://www.tandfonline.com/loi/gmcl17

Brewster Angle Method for Refractive Index Measurements of Biaxial Organic Systems

C. H. Grossman [a] & A. F. Garito [a]

[a] University of Pennsylvania, Department of Physics, Philadelphia, PA

Version of record first published: 04 Oct 2006.

To cite this article: C. H. Grossman & A. F. Garito (1989): Brewster Angle Method for Refractive Index Measurements of Biaxial Organic Systems, Molecular Crystals and Liquid Crystals Incorporating Nonlinear Optics, 168:1, 255-267

To link to this article: http://dx.doi.org/10.1080/00268948908045976

PLEASE SCROLL DOWN FOR ARTICLE

Full terms and conditions of use: http://www.tandfonline.com/page/terms-and-conditions

This article may be used for research, teaching, and private study purposes. Any substantial or systematic reproduction, redistribution, reselling, loan, sub-licensing, systematic supply, or distribution in any form to anyone is expressly forbidden.

The publisher does not give any warranty express or implied or make any representation that the contents will be complete or accurate or up to date. The accuracy of any instructions, formulae, and drug doses should be independently verified with primary sources. The publisher shall not be liable for any loss, actions, claims, proceedings, demand, or costs or damages whatsoever or howsoever caused arising directly or indirectly in connection with or arising out of the use of this material.

Mol. Cryst. Liq. Cryst., 1989, Vol. 168, pp. 255–267
Reprints available directly from the publisher
Photocopying permitted by license only
© 1989 Gordon and Breach Science Publishers S.A.
Printed in the United States of America

Downloaded by [Tomsk State University of Control Systems and Radio] at 12:13 19 February 2013

Brewster Angle Method for Refractive Index Measurements of Biaxial Organic Systems

C. H. GROSSMAN and A. F. GARITO

University of Pennsylvania, Department of Physics, Philadelphia, PA

(*Received August 7, 1988*)

A highly sensitive and convenient Brewster angle method is reported for the accurate determination of the refractive index values for a biaxial crystal. The method is demonstrated for the near infrared through visible spectral ranges with the biaxial organic crystal MNA (2-methyl-4-nitroaniline) well known for its large nonlinear optical coefficients.

INTRODUCTION

Reflectance measurements based on the Brewster condition provide a highly sensitive and convenient method for determining the refractive index and extinction coefficient of isotrophic[1] and uniaxial[2] media. No absolute reflectance measurements are required, and usually, only as few as two reflectance related parameters need be measured. Importantly, these parameters can be obtained with high accuracy using standard techniques. Thus, the Brewster angle can be easily measured with accuracy of $\pm\ 1 \times 10^{-2}$ degrees and reflectance ratios of $\pm\ 1 \times 10^{-3}$ which yield refractive index values to within $\pm\ 1 \times 10^{-3}$.

In this paper, we report a highly accurate method for determining the refractive indices of transparent biaxial media. With $k = 0$, the Brewster angle for combinations of principal optical axes is determined from measurements of the angular dependence of the reflectance whose electric field vector lies in the plane of incidence. Only two crystal faces are required in order to obtain three biaxial Brewster angles and corresponding refractive indices.

The method is experimentally demonstrated for the biaxial organic crystal MNA (2-methyl-4-nitroaniline) using three fixed laser wavelengths in the sample transparency range from the near infrared through visible regions. MNA is an important case in nonlinear optics and electrooptics because of its large nonresonant second order nonlinear optical coefficients.[3,4] The refractive indices of MNA are required for both understanding the microscopic electronic origins of the nonlinear properties and various optical calculations.

BREWSTER ANGLE METHOD

In an anisotropic biaxial medium, the standard relation between the electric displacement **D** and the electric field **E** in the principal coordinate system is diagonal;

$$\mathbf{D} = \begin{bmatrix} \epsilon_x & 0 & 0 \\ 0 & \epsilon_y & 0 \\ 0 & 0 & \epsilon_z \end{bmatrix} \mathbf{E} \tag{1}$$

where in the transparent region of the crystal, the components of the dielectric tensor can be written $\epsilon_i = n_i^2$. The electric field amplitude of light reflected from an oriented crystal face and polarized in the plane of incidence (see Figure 1) is derived in Appendix A,

$$E_r\left(\sqrt{1 - \left(\frac{\sin\theta}{n_\perp}\right)^2} + n_\parallel \cos\theta\right) = E_i\left(\sqrt{1 - \left(\frac{\sin\theta}{n_\perp}\right)^2} - n_\parallel \cos\theta\right). \tag{2}$$

where $n_\parallel$ is the index along the principal axis that is in the face of the crystal and in the plane of incidence, and $n_\perp$ is the index along the principal axis perpendicular to the crystal face. The Brewster condition occurs when Equation 2 vanishes, that is,

$$1 - \left(\frac{\sin\theta}{n_\perp}\right)^2 = n_\parallel^2 \cos^2\theta. \tag{3}$$

There are six possible geometries, each giving different Brewster angles, *nx-ny* ($n_\parallel$-$n_\perp$), *nx-nz*, *ny-nx*, *ny-nz*, *nz-nx*, and *nz-ny*. Of course, only three of these are needed, but choosing the suitable three of the six combinations is important. For example, by defining the following Brewster angles: *ny-nz* (giving θ_1); *nz-ny* (θ_2);

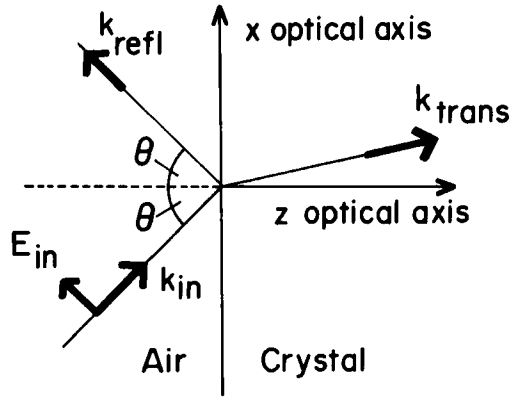

FIGURE 1 Boundary for the Brewster angle experiment showing the optical axes and incident polarization.

Downloaded by [Tomsk State University of Control Systems and Radio] at 12:13 19 February 2013

nx-ny (θ_3), notice that θ_2 and θ_3 can both be measured from the same Y-cut crystal face and the following simple relations hold,

$$n_y^2 \cos^2\theta_1 = 1 - \left(\frac{\sin\theta_1}{n_z}\right)^2 \tag{4}$$

$$n_z^2 \cos^2\theta_2 = 1 - \left(\frac{\sin\theta_2}{n_y}\right)^2 \tag{5}$$

$$n_x^2 \cos^2\theta_3 = 1 - \left(\frac{\sin\theta_3}{n_y}\right)^2 . \tag{6}$$

Combining Equation 4 and Equation 5 gives;

$$n_z = \frac{\sin\theta_1}{\cos\theta_2} \tag{7}$$

$$n_y = \frac{\sin\theta_1}{\cos\theta_2} . \tag{8}$$

Rewriting Equation 6 gives;

$$n_x = 1 + \left(1 - \frac{1}{n_y^2}\right) \tan^2\theta_3 \tag{9}$$

The simplicity of these relations greatly reduces the error propagation from experimental uncertainty in each θ_i to the uncertainty in the indices. Errors of about 0.1–0.2 percent for θ_B propagate into errors of about 0.2–0.4 percent for the index. A statistical curve-fitting procedure[5] is used to accurately derive the value of θ_i from the reflectivity data. The parameters of the reflectivity function are adjusted to best fit the data, and the error in each parameter is determined from the standard deviation of the fit. As shown in Appendix B, the reflectivity near the Brewster angle can be written in a simple parametric form,

$$R(\theta) = \left(\frac{E_r}{E_i}\right)^2 = A^* \frac{(\sin^2\theta - \sin^2\theta_i)^2}{(\cos^2\theta_i \cos^2\theta)^2} + B \tag{10}$$

where the values for the parameters A, B, and θ_i are determined from the χ^2 statistical fitting procedure. A typical example of the reflectivity data and curve fitting is shown in Figure 2 for the reflected intensity as a function of angle near the Brewster angle θ_3 at the wavelength 0.600 μm.

EXPERIMENTAL PROCEDURE AND RESULTS

The experimental layout for the Brewster angle measurements is shown in Figure 3. The output of a continuous wave laser source is focused onto an oriented crystal

Downloaded by [Tomsk State University of Control Systems and Radio] at 12:13 19 February 2013

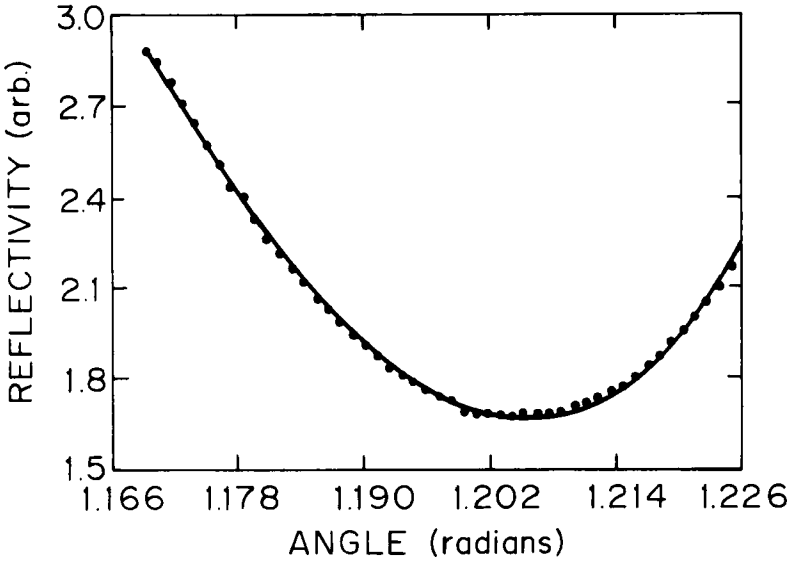

FIGURE 2 A plot of the reflection data and the fitted reflectivity curve from Equation 10. Fitting the theoretical curve gives the Brewster angle as a parameter with standard deviation.

and the reflection is detected. Fixed wavelength lines at 1.064, 0.600, and 0.514 μm are provided by cw Nd:YAG, argon ion pumped dye, and argon ion lasers, respectively. The incident power must be sufficiently high for the weak reflections near the Brewster angle to be detected above the background noise. The typical powers used are 100 milliwatts, which is easily attained with commercial lasers. When focused onto the sample, the intensity is approximately 200 W/cm^2.

The incident beam is polarized and chopped while being monitored for power fluctuations. In Figure 3, a glass slide (1) splits off 5–10% of the laser output for monitoring at the photodiode (6). The remaining light is then polarized in the plane

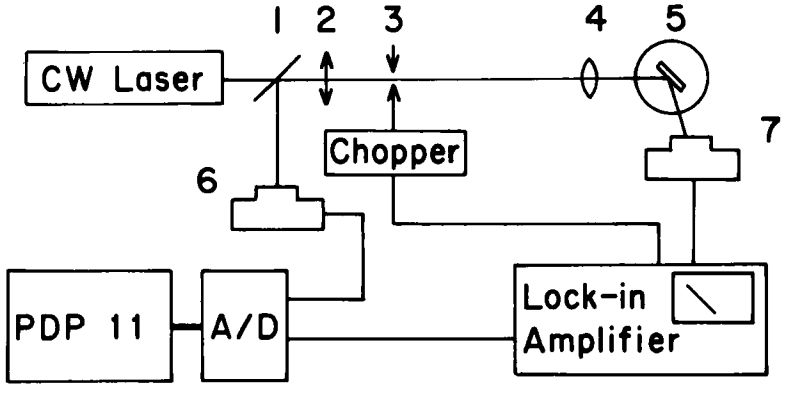

FIGURE 3 Brewster angle experimental setup. Different lasers are used to produce several wavelengths.

Downloaded by [Tomsk State University of Control Systems and Radio] at 12:13 19 February 2013

of incidence with a Nicol prism (2) and modulated with a rotating chopper blade (3) to a frequency ≈100 hz. The chopper controller sends a synchronized pulse to the lock-in amplifier. The light beam is then focused onto the crystal surface with a 10 cm focal length lens (4).

The orientation and control of the crystal position must be of high accuracy. A crystal, cut and polished with two of its optical axes in the input face, is held and oriented with goniometer head, which has two rotation and three translation adjustments. The goniometer head is mounted on a stepper motor-driven rotation stage with a resolution of 120 steps per degree. Great care is taken to ensure that the rotation axis of the stage is in the crystal face and that the light beam strikes the surface along this axis. In order to orient vertically one of the principal axes of the crystal, a Nicol prism analyzer is placed after the stage, and the crystal is positioned normal to the beam. With the polarizer and analyzer crossed, the crystal orientation is then adjusted to extinguish the laser light.[6] Once properly aligned, the stage position counter is set to zero at the approximate position of normal incidence.

The detection system consists of a chopper, a lock-in, and two photodiodes,, as shown in Figure 3. One photodiode (6) monitors the laser power fluctuation before the chopper. The second photodiode (7) detects the reflected power. Its signal is measured by a lock-in amplifier, which stabilizes low power signals and eliminates noise due to stray room light. This detection system allows accurate readings of very low reflectivities close to the Brewster angle. The laser power signal from the photodiode (6) and the output of the lock-in are sent to an A/D converter in a PDP11 computer. The computer divides the laser power signal into the reflected power signal to eliminate any effects of laser power fluctuations. One data point consists of the average over 10 readings.

The Brewster angle is the angle between the crystals position of zero reflection and the position of normal incidence. This poses the experimental problem of accurately determining the position of normal incidence to within at least 0.1 degrees. Usually, one measures the maximum backreflection through a pinhole to determine normal incidence. The accuracy of this method is questionable for two reasons. One reason is that the pinhole alters the intensity profile of the beam cross section and even the direction of the incident light. Secondly, as the back reflection passes through the lens, the transmitted intensity through the pinhole does not drop off sharply with angle. In order to reduce error in the curve fitting procedure for the transmitted back reflected intensity, a detailed analysis of the transmission of a focused beam through a pinhole as a function of angle is desired. These difficulties can be overcome by measuring two Brewster angles, one on each side of normal incidence, to determine the position of normal incidence.

To find each Brewster angle, the sample is rotated about the vertical axis until the reflection vanishes. The reflected intensity is measured and recorded as a function of angle near this first Brewster angle. The crystal is then rotated to the second Brewster position and, again, the reflected intensity is measured as a function of angle. The value for the Brewster angle is one half the angle between these two positions. Thus, by symmetry, the origin is determined from the Brewster positions.

Downloaded by [Tomsk State University of Control Systems and Radio] at 12:13 19 February 2013

Downloaded by [Tomsk State University of Control Systems and Radio] at 12:13 19 February 2013

Crystals of MNA were grown from solution by a method of differential solubility, reported elsewhere.[7] With this method, the crystals form thick plates with typical dimensions of 10 × 10 × 5 mm^3. As determined from x-ray precession camera data[3] and extinction measurements under an optical polarizing microscope, the principal X and Z axes are located in the as-grown (010) face while the Y axis is normal. The principal X axis is approximately parallel ($\approx \pm 1°$) to a natural cleavage plane, which allows easy identification of the axes. Optical transmission measurements show that MNA is transparent from 0.5 to 2.0 μm.[3,4,8]

The Z-cut crystal face for measuring θ_1 was prepared using a solvent string saw and the resulting face was ground and polished with alumina polishing powder. The as-grown crystal face for measuring θ_2 and θ_3 was also polished flat. The back surface was not polished on either crystal so that no strong reflections off the back surface would interfere with the front surface reflection measurements.

Upon fitting the data at the three laser wavelengths, 1.064, 0.600, and 0.514 μm, our measurements yield the Brewster angles listed in Table I. These values are used in Equations 7–9 to calculate the corresponding refractive index values listed in Table II. Previous measurements,[4] using an undefined transmission method, yielded consistently lower values for n_x and n_y, and no n_z values were reported.

DISCUSSION

The measured refractive index values for MNA show a large birefringence. Over the measured transparency range from the near infrared through the visible wavelengths, the refractive index n_x along the principal X axis is much larger than n_y and n_z (Table II and Figure 3). The optical properties of MNA are currently understood in terms of a microscopic electronic description of highly charged correlated excitations in polar aligned structures,[9] and large value of n_x and the birefringence can be understood in terms of this local field model. The square of the refractive index is related to the principal dielectric susceptibility tensor χ_{ij} which can be generally expressed in terms of the microscopic molecular polarizability α_{ij}

$$\chi_{ij} = N \sum_s R^s_{j'j}\, \alpha^{s,\omega}_{j'k'}\, f^{s,\omega}_{k'i'}\, R^s_{ii'} \tag{11}$$

where N is the number of unit cells per unit volume; the sum is over molecules within the unit cell; the matrix $\mathbf{R}^s$ is the rotation matrix from the principal coordinate system to that of molecule of type s; and $\mathbf{f}^{s,\omega}$ is a local field correction at the position of molecule s at the frequency ω. The microscopic dielectric polarization of an

TABLE I

Brewster angles

Wavelength	θ_1	θ_2	θ_3
1.064 μm	62.99° ± 0.04°	51.85° ± 0.06°	65.66° ± 0.11°
0.600 μm	63.88° ± 0.01°	51.87° ± 0.04°	69.44° ± 0.02°
0.514 μm	65.15° ± 0.03°	51.71° ± 0.002°	71.86° ± 0.009°

TABLE II

Refractive index values at several wavelengths

Wavelength	n_x	n_y	n_z
1.064 μm	2.063 ± 0.006	1.732 ± 0.003	1.441 ± 0.002
0.600 μm	2.426 ± 0.003	1.787 ± 0.002	1.454 ± 0.001
0.514 μm	2.764 ± 0.002	1.866 ± 0.003	1.4641 ± 0.0005

MNA molecule is principally aligned along the dipolar molecular x-axis.[10] The MNA dipolar molecules crystallize in a monoclinic unit cell with a noncentrosymmetric space group C_C and point group m as shown in Figure 4.[3] The X principal axis is the vector formed by the average of the microscopic x dipolar axes and corresponds to a crystal polar axis.[3] Because of the polar alignment of the individual molecular dipolar axes along the X direction, each individual molecular microscopic polarization adds constructively in the crystal, and the largest dielectric response is observed along the X principal direction. The crystal optical Z axis is normal to the molecular planes. Since there is very little electronic response out of the molecular plane, the values for n_z are relatively small. Correspondingly, the optical Y axis is in the planes of the molecular sites but is not very close to the molecular x axis. Therefore, its value is expected to be larger than n_z but not as large as n_x. An analysis in terms of calculated local fields and microscopic polarizabilities for Equation 11 is being completed and will be reported separately.

The refractive index values for MNA are required for the calculation of optical properties such as the conditions for phase matched second harmonic generation (PMSHG) in bulk crystals and in waveguide configurations. These calculations require the refractive index values at wavelengths in addition to those at the measured wavelengths. The index dispersion is due to resonant π-electron excitations in the optical absorption region with an edge starting at approximately 0.50 μm. The index values in a transparent region at wavelengths below resonant absorption can be obtained standardly from the Sellmeier equation,[11]

$$n^2 = \mathrm{A3} + \frac{\mathrm{A2}\,\lambda^2}{\lambda^2 - \mathrm{A1}} \tag{11}$$

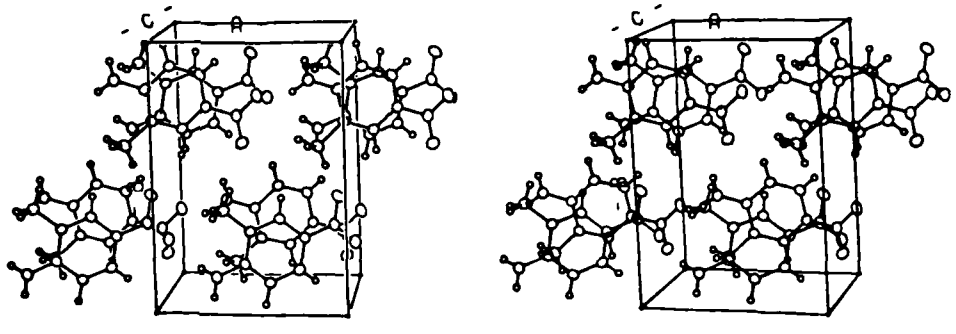

FIGURE 4 Stereoscopic perspective of the molecular orientation within the MNA crystal unit cell. The lattice vectors A, B, and C are for the Ia space group, a non-standard setting of Cc.

Downloaded by [Tomsk State University of Control Systems and Radio] at 12:13 19 February 2013

TABLE III

Parameters used in the Sellmeier equations

Axis	A1	A2	A3
X axis	0.151 ± 0.34%	2.86 ± −1.1%	0.954 ± 6.4%
Y axis	0.185 ± 1.3%	0.223 ± −3.5%	2.733 ± 0.71%
Z axis	0.115 ± 0.18%	0.09 ± −36.0%	1.971 ± 1.4%

where the parameters A1, A2, and A3 are calculated from the index values at three different wavelengths. The parameters are listed in Table III and provide the dispersion curves for n_x, n_y, and n_z as shown in Figure 5.

Thus, for second harmonic generation with a fundamental input at 1.064 μm, for example, the values of n_x, n_y, and n_z obtained at the second harmonic, 0.532 μm, are 2.663 ± 0.006, 1.839 ± 0.005, and 1.46 ± 0.01, respectively. Based on the refractive index values at 1.064 and 0.532 μm, the phase matching angles for MNA crystals have been predicted for Type I PMSHG and shown to agree with the measured PMSHG positions.[12]

Various configurations for achieving PMSHG in nonlinear optical waveguide structures are being actively considered with organic and polymer systems as the nonlinear medium, especialy MNA.[13,14,15] Based on the measured index values, the dimensions of the waveguide can be estimated for phase matching between specific modes as in the example of phase mismatch between two TE modes, with one at the fundamental and the other at the second harmonic frequency. For a

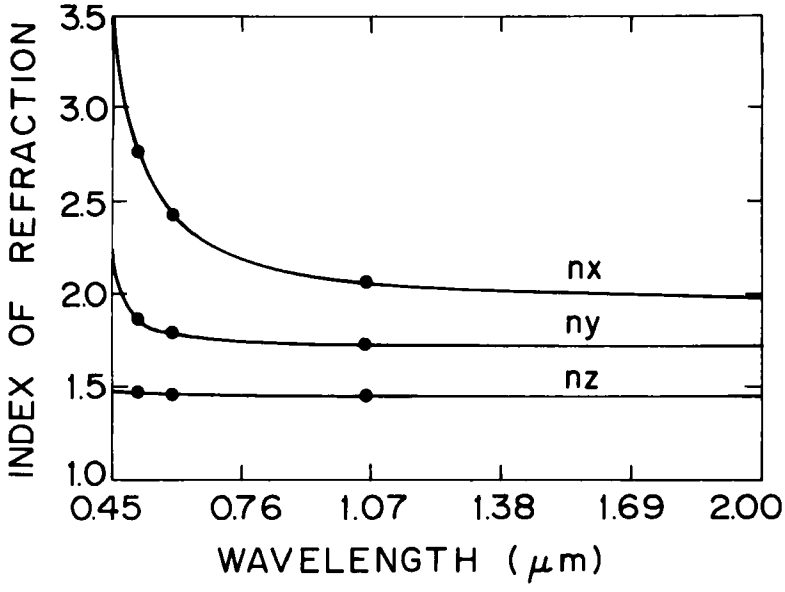

FIGURE 5 The fitted Sellmeier curves for n_x, n_y, and n_z along with the experimental values for the indices at three wavelengths. The real error bars are too small to distinguish the measured values from the curves so asterisks are used in their place.

Downloaded by [Tomsk State University of Control Systems and Radio] at 12:13 19 February 2013

three layered waveguide with the inside layer being MNA, the wave vector β_m for propagation mode m is calcuated from the expression[16]

$$pd - m\pi = \mathrm{Tan}^{-1}\left[\frac{s + q}{p(1 - sqp^{-2})}\right] = [0,2\pi] \tag{12}$$

where

$$p^2 = \left(\frac{\omega}{c}\right)^2 n_{wg}^2 - \beta_m^2 \tag{13}$$

$$q^2 = \left(\frac{\omega}{c}\right)^2 n_{sup}^2 - \beta_m^2 \tag{14}$$

$$s^2 = \left(\frac{\omega}{c}\right)^2 n_{sub}^2 - \beta_m^2 \tag{15}$$

and the inverse tangent is assumed to take the principal value between 0 and 2π. The refractive index values of the substrate, superstrate, and waveguide are fixed with the values n_{sub}, n_{sup}, and n_{wg} at a particular frequency, either ω or 2ω. By choosing the proper thickness for the MNA layer, one can obtain phase matching between modes of propagation at the two wavelengths given by the PMSHG condition $2\beta_n(\omega) = \beta_m(2\omega)$, where n and m are the fundamental and the second harmonic modes, respectively. For example, PMSHG between mode 0 at ω, and modes 1 and 2 at 2ω, for fundamental wavelengths in the range 1.0–1.4 μm is plotted in Figure 6. The calculations use the values $n_{sub} = 1.45$ and $n_{sup} = 1.0$ and give an estimated thickness for PMSHG at 1.064 μm of 0.16 μm when $m = 1$ and 0.33 μm when $m = 2$. These thickness values are about 0.7 times smaller than those based on earlier reports of the index values.[13] At present, no crystals this thin have been grown but PMSHG between higher waveguide modes has been observed in melt-grown crystal[14,15] of thickness $\approx$ 0.6–5.0 μm.

CONCLUSION

In conclusion, a highly sensitive and convenient Brewster angle method has been developed for determining the refractive index values for biaxial crystals using as demonstration the highly nonlinear organic single crystal MNA. This method is simple to apply and derives accurate values of the index of refraction. The measured values are required for various optical calculations such as the determination of PMSHG conditions in bulk crystals and in waveguides. MNA is a well-defined example of a biaxial crystal and serves as a prototype nonlinear optical organic system. The refractive indices of MNA are needed for continued development of microscopic electronic models for polar aligned structures important to nonlinear optics and electrooptics. In addition to other crystalline structures, for example,

Downloaded by [Tomsk State University of Control Systems and Radio] at 12:13 19 February 2013

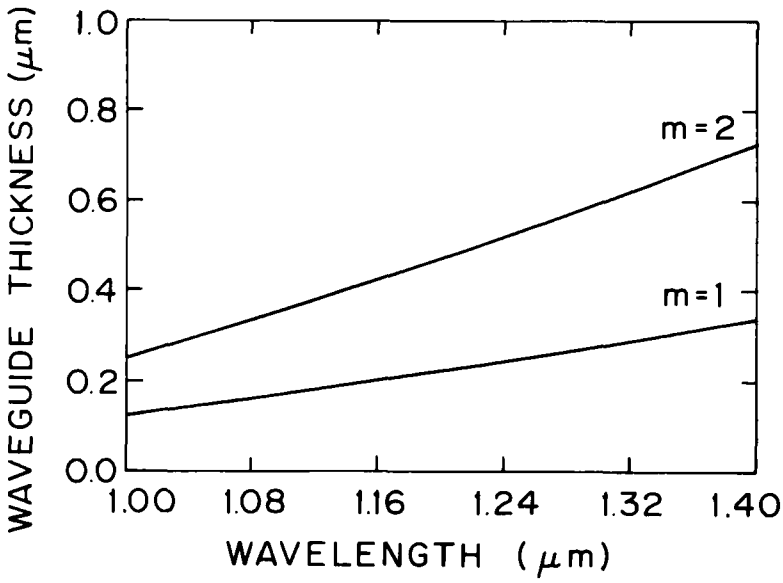

FIGURE 6 The waveguide thickness for PMSHG as a function of fundamental wavelength for MNA. The index m is the mode of the second harmonic propagation in the crystal.

such developments also extend to the nonlinear optical properties of partially ordered polar structures such as poled liquid crystalline phases and molecular doped polymer glasses. The apparent major difference between their diverse polar phases involves their respective orientational distribution functions.

APPENDIX A—REFLECTIVITY OF AN ORIENTED CRYSTAL

For the time being, we choose the axes and interface geometry as shown in Figure 1. We will apply this geometry to other combinations of axes later. The incident field is polarized in the plane of incidence and the incident, reflected, and transmitted electric fields are assumed to be of the form

$$\mathbf{E}_i = E_i(\mathbf{x}\cos\theta - \mathbf{z}\sin\theta)\, e^{i(\mathbf{k}_i\cdot\mathbf{r}-\omega t)} \tag{A.1}$$

$$\mathbf{E}_r = E_r(\mathbf{x}\cos\theta + \mathbf{z}\sin\theta)\, e^{i(\mathbf{k}_r\cdot\mathbf{r}-\omega t)} \tag{A.2}$$

$$\mathbf{E}_t = (\mathbf{x}E_{t,x} + \mathbf{y}E_{t,y} + \mathbf{z}E_{t,z})\, e^{i(\mathbf{k}_t\cdot\mathbf{r}-\omega t)} \tag{A.3}$$

where $\mathbf{x}$, $\mathbf{y}$, $\mathbf{z}$ are unit vectors, and

$$\mathbf{k}_i = \mathbf{x}\, k_i \sin\theta + \mathbf{z}\, k_i \cos\theta \tag{A.4}$$

$$\mathbf{k}_r = \mathbf{x}\, k_r \sin\theta - \mathbf{z}\, k_r\cos\theta \tag{A.5}$$

$$\mathbf{k}_t = \mathbf{x}\, k_{t,x} + \mathbf{z}\, k_{t,z} \tag{A.6}$$

Downloaded by [Tomsk State University of Control Systems and Radio] at 12:13 19 February 2013

At the face z = 0 the equality of the phase factors, $\mathbf{K} \cdot \mathbf{r}$, give $K_{t,i} = 0$ and

$$k_{t,x} = k_i \sin\theta. \tag{A.7}$$

The continuity of electric fields parallel to and displacement fields perpendicular to the interface give the boundary condition

$$E_i \cos\theta + E_r \cos\theta = E_{t,x}, \tag{A.8}$$

$$E_{t,y} = 0, \qquad -E_i \sin\theta + E_r \sin\theta = E_z E_{t,z}. \tag{A.9}$$

From Maxwell's equations, the magnetic fields both inside and outside the medium are derived. Assuming that the medium is nonmagnetic and $\mathbf{H} \sim e^{-i\omega t}$

$$\nabla \mathbf{x} \mathbf{E} = \frac{-1}{c} \frac{\partial}{\partial t} \mathbf{H} = \frac{i\omega}{c} \mathbf{H} \tag{A.10}$$

then from Equation A.1–A.3,

$$\mathbf{H}_i = \frac{c}{\omega} k_i E_i e^{i(\mathbf{k}_i \cdot \mathbf{r} - \omega t)} \mathbf{y}, \tag{A.11}$$

$$\mathbf{H}_r = -\frac{c}{\omega} k_r E_r e^{i(\mathbf{k}_r \cdot \mathbf{r} - \omega t)} \mathbf{y}, \tag{A.12}$$

$$\mathbf{H}_t = \frac{c}{\omega} (E_{t,x} k_{t,z} - E_{t,z} k_{t,x}) e^{i(\mathbf{k}_t \cdot \mathbf{r} - \omega t)} \mathbf{y}. \tag{A.13}$$

The continuity of **H** parallel to the surface at $z = 0$ yields,

$$k_i E_i - k_r E_r = E_{t,x} k_{t,z} - E_{t,z} k_{t,x}. \tag{A.14}$$

Maxwell's equations inside the crystal,

$$\nabla \mathbf{x} \nabla \mathbf{x} \mathbf{E} = \left(\frac{\omega}{c}\right) \mathbf{D} \tag{A.15}$$

results in

$$(\mathbf{x} k_{t,z} - \mathbf{z} k_{t,x})(E_{t,x} k_{t,z} - E_{t,z} k_{t,x}) = \left(\frac{\omega}{c}\right)^2 (\mathbf{x} E_{t,x} \epsilon_x + \mathbf{z} E_{t,z} \epsilon_z)_i . \tag{A.16}$$

Equating each component gives the relation

$$k_{t,x} E_{t,x} \epsilon_x = -k_{t,z} E_{t,z} \epsilon_z . \tag{A.17}$$

Downloaded by [Tomsk State University of Control Systems and Radio] at 12:13 19 February 2013

Substituting $k_{t,x}$ from Equation A.7, $E_{t,x}$ from Equation A.8, $E_{t,z}$ from Equation A.9, and $k_{t,z}$ from Equation A.17 into Equation A.14 gives

$$(E_r - E_i)^2 \left(1 - \frac{\sin^2\theta}{\epsilon_z}\right) = (E_r + E_i)^2 \epsilon_x \cos^2\theta. \tag{A.18}$$

The amplitude E_r is obtained in terms of E_i by taking the negative square root of the left side of A.18 (since $E_r < E_i$) and equating it to the positive square root of the right side A.18. Generalize the coordinate system by calling the x axis the parallel ($\parallel$) axis and the z axis the perpendicular ($\perp$) axis. This makes $\epsilon_x = n_\parallel^2$ and $\epsilon_z = n_\perp^2$. The final equation relating the reflectivity to angle is

$$E_r \left(\sqrt{1 - \left(\frac{\sin\theta}{n_\perp}\right)^2} + n_\parallel \cos\theta\right) = E_i \left(\sqrt{1 - \left(\frac{\sin\theta}{n_\perp}\right)^2} - n_\parallel \cos\theta\right). \tag{A.19}$$

APPENDIX B—REFLECTION CURVE-FITTING ANALYSIS

For more accuracy in determining the Brewster angle from the reflection data, a properly parameterized fitting function is derived. A statistical curve-fitting program[5] is used in fitting the best value for θ_B. To determine a meaningful fitting function, start with Equation 2,

$$E_r (\sqrt{1 - (\sin\theta/n_\perp)^2} + n_\parallel \cos\theta) = E_i (\sqrt{1 - (\sin\theta/n_\perp)^2} - n_\parallel \cos\theta)$$

and the expression for the Brewster condition, Equation 3.

$$\sqrt{1 - (\sin\theta_B/n_\perp)^2} = n_\parallel \cos\theta_B$$

For ease of notation rewrite the reflectivity and the Brewster condition with $n_\parallel^2 = \epsilon_\parallel$ and $n_\perp^2 = \epsilon_\perp$,

$$\frac{E_r}{E_i} = \frac{\sqrt{\epsilon_\perp - \sin^2\theta} - \sqrt{\epsilon_\perp \epsilon_\parallel \cos^2\theta}}{\sqrt{\epsilon_\perp - \sin^2\theta} + \sqrt{\epsilon_\perp \epsilon_\parallel \cos^2\theta}} \tag{B.1}$$

and,

$$\epsilon_\perp - \sin^2\theta_B = \epsilon_\parallel \epsilon_\perp \cos^2\theta_B. \tag{B.2}$$

Combine Equation B.1 and Equation B.2,

$$\frac{E_r}{E_i} = \frac{\cos\theta_B \sqrt{\epsilon_\perp - \sin^2\theta} - \cos\theta \sqrt{\epsilon_\perp - \sin^2\theta_B}}{\cos\theta_B \sqrt{\epsilon_\perp - \sin^2\theta} + \cos\theta \sqrt{\epsilon_\perp - \sin^2\theta_B}} \tag{B.3}$$

Downloaded by [Tomsk State University of Control Systems and Radio] at 12:13 19 February 2013

Equation B.3 is then written as,

$$\frac{E_r}{E_i} = \frac{(\epsilon_\perp - 1)(\sin^2\theta - \sin^2\theta_B)}{\cos^2\theta_B \cos^2\theta\left(\sqrt{\frac{\epsilon_\perp - 1}{\cos^2\theta} + 1} + \sqrt{\frac{\epsilon_\perp - 1}{\cos^2\theta} + 1}\right)} \tag{B.4}$$

Since the term in the denominator within the parentheses varies slowly with small changes in θ, we can treat it as a constant in our analysis. For example, with $\epsilon_\perp = 2.25$, $\theta_B = 60.0°$ and $\theta = 59.0°$ compared to $\theta = 61.0°$, this term is 23.42 and 24.63). To account for any background noise in the data, a constant term is added, giving a reflectivity fitting function:

$$R(\theta) = \left(\frac{E_r}{E_i}\right)^2 = A^* \frac{(\sin^2\theta - \sin^2\theta_B)^2}{(\cos^2\theta_B \cos^2\theta)^2} + B \tag{B.5}$$

References

1. S. P. F. Humphreys-Owen, *Proc. Phys. Soc.*, **77**, 949 (1960).
2. M. Elshazly-Zaghloul and R. M. A. Azzam, *J. Opt. Soc. Am.*, **72**, 657 (1982).
3. G. F. Lipscomb, A. F. Garito, and R. S. Narang, *J. Chem. Phys.*, **75**, 1509 (1981).
4. B. F. Levine, C. G. Bethea, C. D. Thurmond, R. T. Lynch, and J. L. Bernstein, *J. Appl. Phys.*, **50**, 2523 (1979).
5. P. R. Bevington, *Data Reduction and Analysis for the Physical Sciences* (McGraw Hill, New York, 1969) pp. 204–246.
6. F. D. Bloss, *Introduction to the Methods of Optical Crystallography* (Holt, Rinehart and Winston, New York, 1961) pp. 49–60.
7. C. H. Grossman, Ph.D. Thesis, University of Pennsylvania (1987).
8. Y. Tokura, A. Kurita, and T. Koda, *Phys. Rev. B*, **31**, 2588 (1985).
9. See for example, V. M. Agranovich and A. A. Maradudin, *Electronic Excitation Energy Transfer in Condensed Matter* (North Holland, Amsterdam, 1982) p. 59.
10. C. C. Teng and A. F. Garito, *Phys. Rev. B*, **28**, 6766 (1984).
11. B. Tatian, *Appl. Opt.*, **23**, 4477 (1984).
12. OSA Meeting Technical Digest, 1985, and C. H. Grossman and A. F. Garito, "Phase Matched Second Harmonic Generation in Organic Single Crystals of 2-Methyl-4-Nitroaniline", *J. Opt. Soc. B*, submitted.
13. George I. Stegeman and C. Liao, *Appl. Opt.*, **22**, 2518 (1983).
14. K. Sasaki, T. Kinoshita, and N. Karasawa, *Appl. Phys. Lett.*, **45**, 333 (1984).
15. H. Ito, K. Hotta, H. Takara, and K. Sasaki, *Appl. Opt.*, **25**, 1491 (1986).
16. Y. Suematsu, Y. Sasaki, K. Furuya, K. Shibata, and S. Ibukuro, *IEEE J. Quantum Electron.*, **QE10**, 222 (1974).

Downloaded by [Tomsk State University of Control Systems and Radio] at 12:13 19 February 2013